Experimental Mechanics (2012) 52:829–842
DOI 10.1007/s11340-012-9601-9

Assessment of Non-adiabatic Behaviour in Thermoelastic Stress Analysis of Composite Sandwich Panels

D.A. Crump · J.M. Dulieu-Barton

Received: 21 September 2010 / Accepted: 31 January 2012 / Published online: 25 February 2012

Abstract Thermoelastic stress analysis (TSA) is used to derive the surface stresses in large sandwich structure panels with honeycomb core and carbon fibre face sheets. The sandwich panels are representative of those used for secondary aircraft structure. The panels were subjected to a pressure load, similar to that experienced in-service, using a custom designed test rig. To achieve the necessary adiabatic conditions for TSA, cyclic loading is regarded as an essential feature. As the panels were full-scale, the maximum loading frequency that could be imparted to the panels by the rig was 1 Hz, which is below the usual range recommended to achieve adiabatic behaviour. To assess the effectiveness of TSA at low frequencies two approaches to calibration are investigated and compared with the stress distribution obtained from independently validated FE models. The thermoelastic response was calibrated into stress data using thermoelastic constants derived experimentally from tensile strips of the sandwich panel face sheet material. It is shown that by using thermoelastic constants obtained from the tensile strips manufactured with the same lay-up as the sandwich panel face sheets, and at the same cyclic load frequency used in the full-scale tests, quantitative stress metrics can be derived from the TSA data. More significantly, a deeper insight into the importance of the thermal characteristics in TSA of laminated materials is provided. It is demonstrated that, for the material used in this work, it is possible to use the global material behaviour to obtain quantitative results when adiabatic conditions do not prevail.

D.A. Crump (✉) · J.M. Dulieu-Barton
School of Engineering Sciences, University of Southampton,
Highfield,
Southampton SO17 1BJ, UK
e-mail: dac400@soton.ac.uk

Keywords TSA · Calibration · Full scale testing · Composite sandwich

Introduction

Thermoelastic stress analysis (TSA) [1] is a well established non-contacting technique for the evaluation of stresses in engineering components, e.g. [2–5]. The technique uses an infra-red detector to obtain the small temperature change associated with the thermoelastic effect in a loaded component or structure. It is assumed that the small temperature change occurs isentropically; to eliminate heat transfer TSA is usually performed using a cyclic load. TSA has been successfully applied to realistic composite structures, e.g. large wind turbine blades [6] and marine tee-joints [7]. The overall motivation for the work in this paper is to provide a means of assessing the mechanical performance of large sandwich structures produced using different manufacturing processes described in [8]. The aim of the current paper is to demonstrate that TSA can be used as an accurate and quantitative assessment tool for complex sandwich structures with carbon fibre face sheets.

An ongoing thrust of research is the development of TSA as a validation tool for finite element analysis (FEA) of complex composite structures. In [9] TSA was applied to sandwich beams with cores of varying stiffness. At the junction of the cores large stress gradients occur both through the thickness and in the plane of the face sheet. In TSA, it is well known that stress gradients drive non adiabatic behaviour. In the case where the face sheets were manufactured from relatively low thermal conductivity material it was possible to obtain results from the TSA that compared well with strain gauge readings, enabling a full-field validation of the FEA. For high conductivity

aluminium alloy face sheets it was shown that adiabatic conditions could not be achieved because of the large through thickness and in-plane stress gradients at the core junctions. In the present paper, sandwich structures with multidirectional laminated carbon fibre face sheets are studied, which have a much greater thermal conductivity than the glass fibre face sheets used in [9]. The carbon fibre material presents a challenge as the stress-induced temperature change in each ply of the face sheet laminate is different ply-by-ply and therefore at the ply interface there will be a large stress gradient.

The paper starts with a description of the TSA technique and its application to large polymer composite carbon fibre sandwich structure panels representative of a secondary wing structure panel in an aircraft [8]. The panels are subjected to a pressure load, which models the aerodynamic pressure on the wing of an aircraft, using a specialist test rig [10]. The rig imparts comparatively large displacements and limits the loading frequencies to a maximum of 1 Hz. In [11] the loading frequency threshold necessary to achieve adiabatic behaviour in carbon fibre reinforced materials composite materials was investigated. It was noted that 10 Hz is generally considered adequate for homogeneous materials. However due to the heterogeneous nature of composites, in particular laminates with plies of differing orientation, it was recommended that the loading frequency may need to be as much as 30 Hz. The requirement for this relatively high loading frequency limits the use of TSA to laboratory experiments, and also the size of components to which TSA can be readily applied. In conducting full-scale tests there is always a compromise between loading frequency and displacement; hence the work described in the paper is relevant to a wide range of applications where TSA might be applied to realistic structures.

Two different approaches have been suggested for the calibration of the thermoelastic response from laminated polymer composites [12]. The approaches use either, the global mechanical and thermoelastic response of the material, or use the thermoelastic response from the surface ply alone. In the present paper, the calibration approaches are tested over a range of loading frequencies to provide a map of the thermoelastic response of laminated materials. To further illuminate, two numerical model types are used: one that simply treats the face sheet materials as homogeneous blocks and the other where the ply by ply response is considered. The validity of these models is discussed, by comparing with TSA data and the measured maximum deflection of the panels. It is shown that only the model that treats the face sheets as homogeneous blocks can provide correspondence with the thermoelastic data. A detailed discussion explains that when laminated composite structures are loaded at low cyclic frequencies it is inappropriate to calibrate the thermoelastic response from the surface ply alone.

Representative Panels and Experimental Arrangements

In previous work [8], a generic sandwich panel was designed to capture some of the features representative of composite sandwich secondary wing structure (see Fig. 1). The panels were manufactured using a variety of material architectures and processes. Here two generic panels were manufactured using Hexcel's 914 C-TS-5-34% prepreg tape as the face sheet material, one with quasi-isotropic (QI) sheets $[0°, 45°, -45°, 90°, 0°, 45°, -45°, 90°, 0°, 45°, -45°, 90°]_s$ and the other with cross-ply (CP) sheets $[0°, 90°]_{6s}$ about a Nomex honeycomb core. The prepreg tape and autoclave approach was chosen as it is the simplest to control in terms of consistency and also it is possible to manufacture a variety of stacking sequences as required for calibration (see Calibration Approach). The QI and CP laminates were chosen to investigate the effect of bend-twist coupling on the structural response and to provide a straightforward means of assessing heat transfer through the thickness of the face sheets.

A custom designed rig was used to apply a pressure load [10], representative of aerodynamic loading, to the sandwich panel (Fig. 2). The rig used the displacement of the actuator in an Instron servo-hydraulic test machine to pull the sandwich panel over a water filled pressure cushion that is fully constrained by the rig and the panel. The rig was designed to allow uninterrupted optical access to the top surface of the sandwich panel, thereby enabling the use of TSA. The panel was attached to the test rig horizontally, as shown in Fig. 2. The panel was bolted to the test rig on three sides, to be representative of the attachment approach used on aircraft, allowing one of the longer edges free to deflect; full details of the rig design and operation are provided in [10]. First a static load of 10 kPa (1.5 psi) was applied to each panel and a LVDT displacement transducer was used to measure the maximum out-of-plane deformation. Then the panels were loaded cyclically at 1 Hz with a mean pressure of 10 kPa (1.5 psi) and an amplitude of 5 kPa (0.75 psi), thereby imparting a pressure range of 10 kPa (1.5 psi) for the TSA.

Thermoelastic Stress Analysis—Equipment and Theory

A Cedip Silver 480 M infra-red detection system manufactured by Cedip Infrared Systems was used to obtain the TSA data. The system comprises an infra-red camera with a 320× 256 InSb detector array with a pitch of 30 μm and allows frame rates between 5 and 380 Hz. The images are recorded and processed using AltairLI software. The Cedip system is radiometrically calibrated so it is possible to obtain the temperature change directly as well as using the mean temperature field to correct for any changes in the specimen

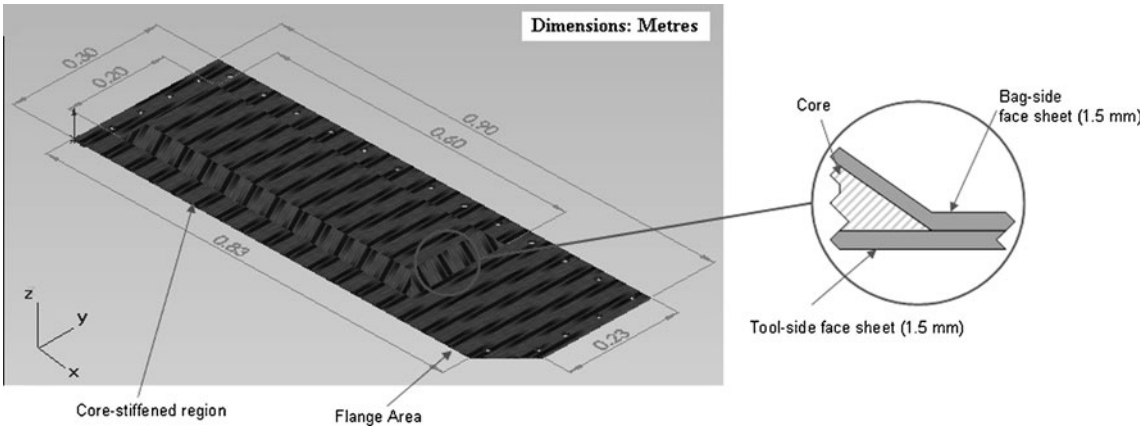

Fig. 1 Generic panel design

temperature. A 'lock-in' signal from the test machine is used to synchronise the TSA measurement, and in this way the thermoelastic response can be averaged over a number of cycles so that the temperature resolution is improved. The output from the detector provides the change in surface temperature, ΔT, resulting from the change in the principal stresses on the surface of the material. The specimens were not coated with paint as the response was sufficient in the uncoated condition. To obtain the thermoelastic response from the surface it was necessary to mount the infra-red camera vertically with the lens directed downwards. The detector was located at a distance that gave approximately 600 pixels across the 300 mm width of the panel. Therefore, the spatial resolution was approximately 2 pixels/mm and the system recorded images at a frame rate of 100 Hz. Each TSA measurement was produced by recording and processing across 1000 images. To achieve the spatial resolution for the entire panel it was necessary to record 32 sets of images per panel, and then 'stitch' the data together using a Matlab routine to provide a full-field plot of the temperature change on the surface of the sandwich panels.

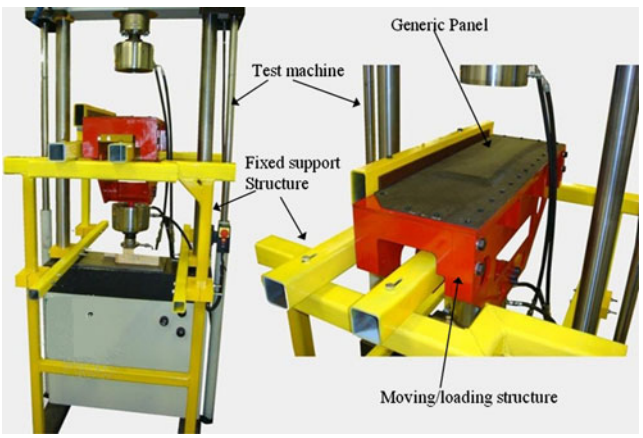

Fig. 2 Pressure rig attached to test machine

For an orthotropic material, such as the composite face sheet material investigated in this paper, ΔT can be related to the stresses in the material as follows [7]:

$$\Delta T = \frac{-T}{\rho C_p}\left(\alpha_x\sigma_x + \alpha_y\sigma_y + \alpha_{xy}\sigma_{xy}\right) = \frac{-T}{\rho C_p}\left(\alpha_1\sigma_1 + \alpha_2\sigma_2\right) \quad (1)$$

where σ_1 and σ_2 are the stresses in the principal material directions, σ_x and σ_y are the direct stresses in any arbitrary direction, σ_{xy} is the shear stress, α_1 and α_2 are the coefficients of linear thermal expansion in the principal material directions and α_x, α_y and α_{xy} are the coefficients of linear thermal expansion in the same arbitrary stress directions, ΔT is the change in temperature, T is the ambient temperature, ρ is the density and C_p is the specific heat at constant pressure.

It is important to note that as ΔT is a scalar quantity the thermoelastic response is independent of the co-ordinate system that is being used to analyse the stresses; this is illustrated by (equation (1)) and demonstrated in [13, 14]. However, in laminated composite materials the reference axes can either be related to an individual ply orientation or to the entire stack (i.e. global values). In the current work the surface ply longitudinal and transverse axes are aligned to the x and y direction respectively, and the principal laminate axes are also in the x-y direction as shown in Fig. 1. Therefore throughout the paper the reference axes will be the x-y axes, which are the principal material axes for the surface ply and the laminate; hence the shear term in (equation (1)) can be neglected. Therefore considering the x-y co-ordinate system only in (equation (1)) it is possible to combine the material constants, i.e. α_x, α_y, ρ and C_p into two thermoelastic constants K_x and K_y as follows [10]:

$$\Delta T = -T\left(K_x\sigma_x + K_y\sigma_y\right) \quad (2)$$

where $K_x = \frac{\alpha_x}{\rho C_p}$ and $K_y = \frac{\alpha_y}{\rho C_p}$.

This allows (equation (2)) to be rearranged so that a stress metric is obtained where the measured ΔT can be

calibrated in such a way that it can be used for FEA validation:

$$\underbrace{\frac{\Delta T}{TK_x}}_{TSA} = \underbrace{\Delta\sigma_x + \frac{K_y}{K_x}\Delta\sigma_y}_{FE} \tag{3}$$

The left hand side of (equation (3)) represents the calibration of ΔT into a stress metric and the right hand side into the form that the FE data must be processed to make it comparable with the TSA data. Therefore a means of deriving the thermoelastic constants must be established.

Calibration Approach

One of the major challenges in calibrating the thermoelastic response from composite materials is the requirement for accurate thermal and mechanical material properties both longitudinally and transversely. By using (equation (2)) it is possible to calibrate the thermoelastic response using measured thermoelastic constants K_x and K_y. The uniaxial stress state in a tensile strip test provides the opportunity to experimentally obtain the thermoelastic constants by using specimens orientated in the material longitudinal and transverse directions it is possible to calculate K_x and K_y as follows:

$$K_x = \frac{-\Delta T}{\Delta\sigma_x T} \text{ and } K_y = \frac{-\Delta T}{\Delta\sigma_y T} \tag{4}$$

Two calibration approaches are investigated to establish if the stresses in (equations (2) and (3)) should be the global (laminate) stresses or surface ply (lamina) stresses in the face sheet. The key feature is to determine if this has an effect on the interpretation of the thermoelastic response. The first, 'global calibration', uses constants derived from tensile strips manufactured from material with the same stacking sequence as the face sheets of the generic panel, i.e. QI and CP depending on the panel. The second, 'UD calibration', uses constants derived from tensile strips manufactured with a unidirectional lay-up, i.e. all plies aligned longitudinally or transversely. As the surface ply in the panel face sheets is orientated with the x-direction (see Fig. 1) for all panels, the surface ply thermoelastic constants derived from the UD strips can be applied to both the QI and CP generic panels.

Tensile strips of 15 mm width were loaded in a servo-hydraulic test machine at 1, 2, 5, 10, 15 and 20 Hz to investigate the effect of loading frequency on the derived thermoelastic constant. As a result of the different stiffness and strengths of the materials it was necessary to apply different loads to the longitudinal and transverse UD specimens than that used for the QI and CP strips. The longitudinal UD specimen was loaded at 10±9.0 kN, the transverse UD specimen at 0.15±0.1 kN whilst all the QI and CP specimens were loaded at 3.5±3.0 kN.

Tables 1, 2 and 3 provide the average ΔT value obtained from each of the tensile strips, taken from an area comprising 15000 and 20000 data points, at all the loading frequencies; T and global applied stress change, σ, are also given in the tables. The standard deviation of the ΔT and T values are also included to give an indication of the noise in the measurement. The noise content of the ΔT measurements is high; standard deviations are of the same order as the

Table 1 Temperature change for the UD tensile specimens

UD 0°: σ_x=187.5 MPa				
Frequency (Hz)	ΔT (°K)	Standard Error ΔT (x 10^{-5})	T (°K)	Standard Error T (x 10^{-4})
1	0.0175±0.0107	7.54	294.0±0.0603	4.25
2	0.0159±0.0109	7.68	294.1±0.0744	5.24
5	0.0186±0.0115	8.10	297.8±0.1030	7.26
10	0.0197±0.0122	8.60	294.0±0.0495	3.49
15	0.0203±0.0120	8.45	297.9±0.1050	7.40
20	0.0206±0.0123	8.67	297.9±0.0976	6.88
UD 90°: σ_y=4.17 MPa				
Frequency (Hz)	ΔT (°K)	Standard Error ΔT (x 10^{-5})	T (°K)	Standard Error T (x 10^{-3})
1	0.0235±0.0058	5.06	295.1±0.1170	1.02
2	0.0242±0.0062	5.41	295.4±0.1070	0.93
5	0.0247±0.0062	5.41	295.5±0.1049	0.91
10	0.0247±0.0065	5.67	295.5±0.1066	0.93
15	–	–	–	–
20	–	–	–	–

Table 2 Temperature change for the QI tensile specimens

QI 0°: σ_x=122.75 MPa				
Frequency (Hz)	ΔT (°K)	Standard Error ΔT (x 10^{-4})	T (°K)	Standard Error T (x 10^{-3})
1	0.0576±0.0300	2.40	295.6±0.0780	0.62
2	0.0478±0.0258	2.06	294.8±0.0641	0.51
5	0.0419±0.0200	1.60	295.4±0.1586	1.27
10	0.0351±0.0191	1.24	295.6±0.0729	0.48
15	0.0294±0.1890	1.51	295.4±0.0908	0.73
20	0.0275±0.0196	1.57	295.4±0.0719	0.58
QI 90°: σ_y=125 MPa				
Frequency (Hz)	ΔT (°K)	Standard Error ΔT (x 10^{-4})	T (°K)	Standard Error T (x 10^{-4})
1	0.1161±0.0412	3.29	298.5±0.0875	6.99
2	0.1144±0.0390	3.12	298.5±0.0873	6.98
5	0.1306±0.0386	3.08	298.5±0.0825	6.59
10	0.1388±0.0432	2.74	298.5±0.0855	5.42
15	0.1405±0.0492	3.12	298.5±0.0889	5.63
20	0.1404±0.0512	3.24	298.5±0.0820	5.20

mean response. However, much of this noise can be explained by the surface roughness of the composite specimens resulting from the peel ply indentation leading to variation in the emissivity. It should also be noted that ΔT is of the order 20 mK and close to the minimum resolvable value of about 4 mK quoted by the manufacturer. ΔT was small for UD 0° material despite the large applied stress because the α_x value is small and the applied stress had to be small for the UD 90° material to prevent failure during the tests. The noise in the laminated specimens with a transverse surface ply is lower, closer to 30% of the response. However, the average ΔT is obtained from a large number of pixels therefore the confidence in the result is high. To confirm the confidence of the results standard error is also included in Tables 1, 2 and 3; in all cases the standard error is small. The ΔT and T at each loading frequency and the global σ are used to calculate the thermoelastic constant for each specimen at each loading frequency using (equation (4)). The thermoelastic constants for the QI and CP specimens are plotted in Fig. 3. For QI and CP specimen there is a considerable difference between the measured response at 1 Hz and 10 Hz; this is expected, as there is a step change in the stresses ply by ply and hence large stress gradients between

Table 3 Temperature change for the CP tensile specimens

CP 0°: σ_x=124.56 MPa				
Frequency (Hz)	ΔT (°K)	Standard Error ΔT (x 10^{-4})	T (°K)	Standard Error T (x 10^{-4})
1	0.0710±0.0398	2.49	295.0±0.0630	4.15
2	0.0698±0.042	2.52	293.4±0.0666	4.17
5	0.0656±0.0395	2.47	293.4±0.0675	4.23
10	0.0643±0.0396	2.48	295.0±0.0688	4.31
15	0.0517±0.0088	0.69	296.0±0.0527	4.10
20	0.0483±0.0087	0.68	296.2±0.0421	3.28
CP 90°: σ_y=131.06 MPa				
Frequency (Hz)	ΔT (°K)	Standard Error ΔT (x 10^{-4})	T (°K)	Standard Error T (x 10^{-4})
1	0.0783±0.0302	1.99	295.0±0.0816	5.37
2	0.0854±0.0325	2.14	293.9±0.0650	4.28
5	0.0917±0.0333	2.19	293.8±0.0706	4.65
10	0.0991±0.0341	2.24	295.0±0.0761	5.01
15	0.1022±0.0166	1.35	297.3±0.0327	2.65
20	0.1043±0.0170	1.38	297.3±0.0339	2.75

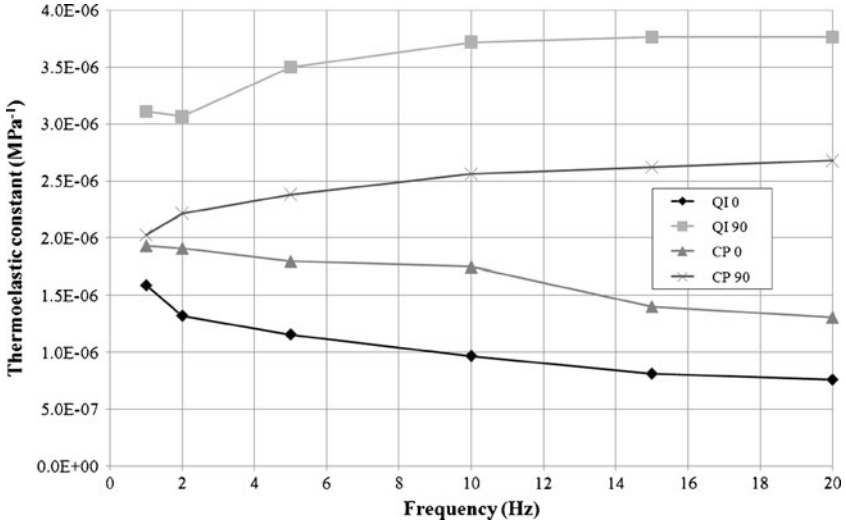

Fig. 3 Variation in thermoelastic constants for QI and CP specimens with frequency

the plies in these specimens. It is evident that as the loading frequency is increased, and conditions become more adiabatic, the thermoelastic constant for each specimen tends towards a uniform value. When the surface ply is orientated at 90° to the line of action of the applied load there is an increase in response as adiabatic behaviour is achieved. Conversely there is a decrease in response as adiabatic behaviour is achieved for the specimens with a 0° surface ply. This indicates that the heat transfer direction is from the 90° ply into the 0° ply. For the QI specimens at 1 Hz the longitudinal specimen provides a K_x value around 50% less than that for the transverse specimen. At 10 Hz K_y is more than three times greater. It is clear that at a 1 Hz loading frequency the QI specimens are not behaving adiabatically because of through thickness heat transfer from the subsurface plies. The response from the transverse specimen becomes uniform at a lower loading frequency than the longitudinal specimen. The K_y values are almost constant at frequencies of 10 Hz and above, whilst it is necessary to increase the loading frequency to between 15 and 20 Hz to obtain the same uniform response for K_x. Finally, for the CP specimens at 1 Hz the K_x value is practically the same as the transverse. Here it could be speculated the heat transfer through the thickness produces an almost homogeneous material where the orientation of the surface ply is unimportant. When the loading frequency is increased to 10 Hz the K_y value is almost two times greater than the longitudinal in a very similar manner to the QI. The presence of ±45° plies in the QI specimen may be responsible for reducing the homogenising effect of heat transfer at low loading frequencies. There is clear non-adiabatic behaviour at 1 Hz for the materials that comprise the panel face sheets. As the loading rig can only operate at this level, then it must be established if applying the thermoelastic constants derived from these loading frequencies will provide a sufficiently accurate stress solution.

Figure 4a and b plot the variation in thermoelastic constant with loading frequency for the longitudinal and transverse UD specimens respectively. The longitudinal UD specimen provides a response that is almost sixty times smaller than the transverse UD specimen, which is consistent with the ratio of the coefficients of thermal expansion for carbon epoxy polymer composites. The derived thermoelastic constants (see Fig. 4) show increases in the response between the 1 and 10 Hz loading frequency of 12% for the UD 0° specimen and 5% for the UD 90° specimen. As all the plies are aligned in the same direction there is no through thickness stress gradient and hence little heat transfer. The small changes in response may be caused by the stress gradient between the surface resin rich layer and fibre reinforced substrate, which has been noticed in previous research [13–15]; this will be further discussed later in this section. Between 10 and 15 Hz there is a smaller increase of around 3% and with little change between 15 and 20 Hz indicating that the possible effect of the resin layer has been eliminated. However, for the UD 90° specimen the response is uniform even at 10 Hz with no change between 5 and 10 Hz. In the UD 90° specimen, the stress is predominately carried by the resin and therefore the expectation is that the stress induced temperature change will be more uniform throughout the specimen.

It is interesting that the thermoelastic constants derived for the QI and CP materials are not the same as those derived for the UD materials. This is because the global applied stress has been used to determine the thermoelastic constants for the QI and CP materials. Hence it is necessary to establish if using the stress in the surface ply alone, of the QI and CP specimens, would provide thermoelastic constants that were comparable to those for the UD material. Classical laminate theory (CLT) [16] was used to calculate the stress state in the surface ply of the QI and CP lay-ups, with both 0° and 90° plies on the surface. When the surface ply is treated in isolation the stress state cannot be assumed to be uniaxial. Poisson's ratio effects from subsurface plies induce transverse stress that must be accounted for when calculating the thermoelastic constants. Table 4 lists

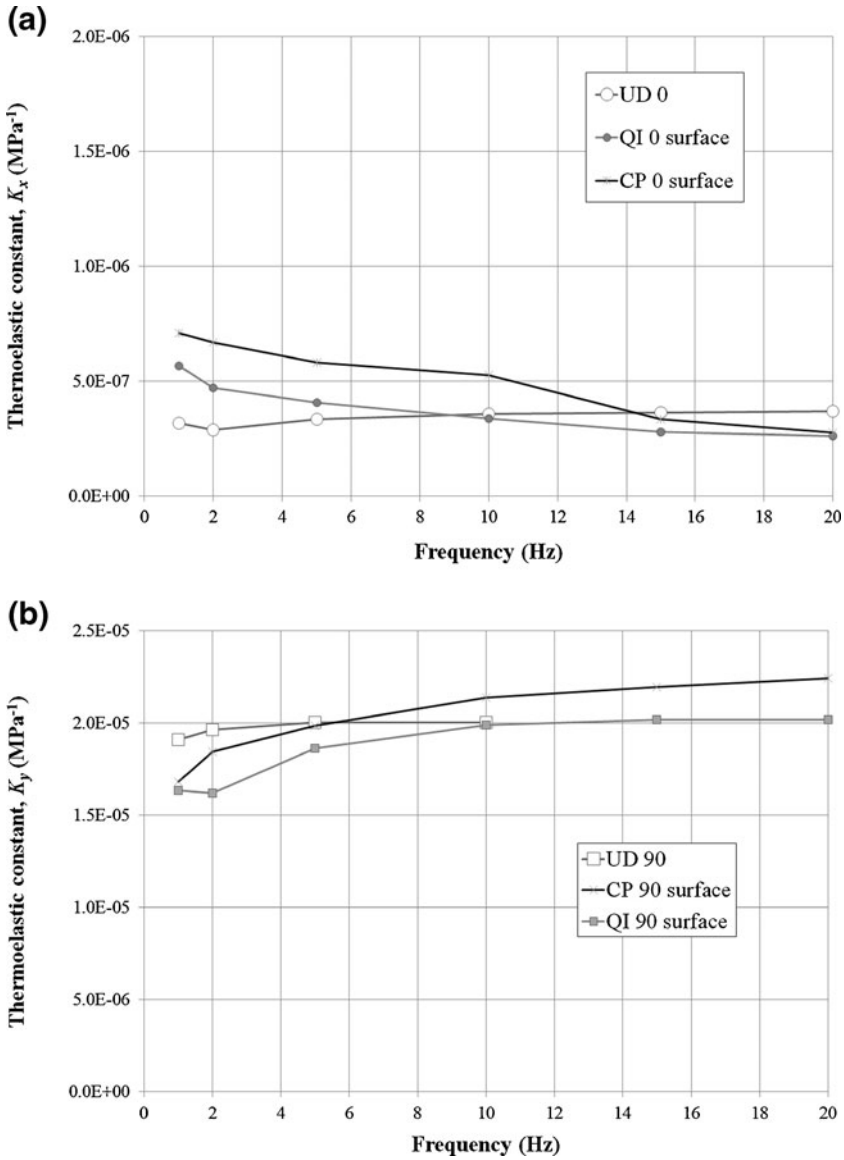

Fig. 4 Variation in thermoelastic constant with frequency for specimens with (**a**) 0 surface ply (**b**) 90 surface ply

values of σ_x and $\underline{\sigma_y}$ for the surface ply of the four specimens obtained using the CLT, i.e. QI 0°, QI 90°, CP 0° and CP 90°. Populating (equation (2)) for CP 0° and CP 90° provides a pair of simultaneous equations with two unknowns:

$$\begin{aligned} &\text{CP } 0^{\circ}: \ \Delta T = T\left(235K_x + 4.4K_y\right) \text{ and} \\ &\text{CP } 90^{\circ}: \ \Delta T = T\left(4.4K_x + 15.6K_y\right) \end{aligned} \tag{5}$$

where ΔT and T are measured. The equations are solved to find K_x and K_y for the surface ply for the CP laminate. A similar set of simultaneous equations can be formed from the QI 0° and QI 90° specimens to find the surface K_x and K_y of the QI laminate. The variation of the surface ply K_x and K_y with loading frequency are plotted alongside the UD thermoelastic constants in Fig. 4a and b respectively. It can be seen from Fig. 4a that the

Table 4 Comparison of measured temperature changes to those calculated from surface ply stresses and 'resin-rich' surface layer

Specimen	ΔT Expt (°K)	Surface ply stress		ΔT Surface ply calc (°K)	Resin stress		ΔT Resin (°K)
		σ_x (MPa)	σ_y (MPa)		σ_x (MPa)	σ_y (MPa)	
CP 0	0.050	235.0	4.4	0.053	16.8	4.7	0.154
CP 90	0.100	15.6	4.4	0.096	17.0	4.8	0.156
QI 0	0.030	336.0	0.3	0.039	20.4	0.2	0.146
QI 90	0.140	96.0	23.0	0.150	26.0	1.4	0.196

UD K_x value is fairly uniform over the frequency range. In contrast to the K_x value obtained from the global calibration approach both the QI and CP K_x values obtained from the surface ply are very close to that of the UD value. However, both the QI and CP K_x values decrease with loading frequency, tending to the UD value, because as the frequency increases the heat transfer from subsurface plies reduces; at 20 Hz the values are approximately the same. Figure 4b shows the variation of the K_y with loading frequency for the UD specimen along with the K_y values derived from the surface ply of the QI and CP specimens. Similarly to that mentioned above, the UD K_y value tends towards a uniform value of approximately 20×10^{-6} MPa^{-1} at 5 Hz. The QI and CP K_y values both tend towards a constant value with increasing loading frequency, as expected due to reduction in heat transfer. As the loading frequency approaches 10 Hz the QI K_y value matches that of the UD, whilst the CP K_y gradually increases to a value of approximately 22.5×10^{-6} MPa^{-1} at 20 Hz. The K_y calculated from the CP specimens is 10% higher than either the UD or QI value; at present there is not an explanation for this apart from a small experimental error.

To provide a deeper insight into the source of the ΔT values measured by the infra-red camera during the experiments. Equation (1) is used to calculate the theoretical expected ΔT. For all the theoretical calculations T is the measured value, whilst values for density, specific heat capacity and coefficient of thermal expansion are listed in Table 5. Most of the material property values have been referenced from the literature and are indicated in the table. As values of α_x vary considerably according to the literature and α_y do not it was decided to use the ratio of the experimentally derived thermoelastic constants for the UD material and α_y to obtain α_x. The resulting value for α_x is well within the range quoted in the literature, e.g. [15]. To confirm the presence of heat transfer from the subsurface ply to the surface ply in longitudinal QI and CP specimens at lower loading frequencies the ratio of theoretical ΔT from both plies was calculated using stresses derived from CLT. For both the QI and CP specimens the ratio was approximately 0.5, i.e. the expected ΔT from the surface ply is approximately half that expected from the subsurface ply leading to a large temperature gradient and therefore heat transfer.

Table 5 Material properties for thermoelastic signal calculations

Property	Composite	Epoxy resin
Density, ρ (kg/m^3)	1600 [16]	1190 [18]
Specific heat capacity, Cp (J/kg °K)	915 [19]	1280 [18]
Coefficient of thermal expansion, α_x (/°C)	0.54×10^{-6}	37×10^{-6} [20]
Coefficient of thermal expansion, α_y (/°C)	30×10^{-6} [16]	n/a

Finally, it has been suggested previously [13–15] and earlier in this paper that the thermoelastic response from the specimens may be dominated by the surface 'resin-rich' layer. Therefore, to further investigate this, the theoretical ΔT is calculated assuming the stress distribution in the surface ply, and from a 'resin-rich' surface layer. Table 4 lists the individual stresses and the respective ΔT for QI and CP, longitudinal and transverse specimens for both surface ply and 'resin-rich' layer. For comparison, the measured ΔT values, under adiabatic conditions (i.e. at 20 Hz), are also included. There is excellent agreement between the experimental ΔT and the theoretical ΔT calculated using the surface ply stresses. This is particularly encouraging when it is considered that the thermoelastic constant material properties are from the literature. The theoretical ΔT calculated from the 'resin-rich' layer is considerably larger than the experimental values and therefore if the resin layer was responsible for the thermoelastic response it would mask any response from the plies below. The only conclusion is that for the carbon-epoxy material used in the present work the response is a result of the surface ply.

In previous work [5, 15, 17], the subject of the source of the thermoelastic response has been discussed, i.e. is the response from the resin rich layer, the surface ply or a combination of both. As in the current work, in [15] predictions of the thermoelastic response from both the resin rich layer and the surface ply of CFRP laminates were made. It was shown that the prediction from the composite surface ply provided a much closer match to the experimental data than that from the 'resin rich layer'. It is interesting that in [5] and [17] the material used was glass fibre reinforced plastic and the conclusion was that the response was that from the resin rich layer. Glass has a much lower thermal conductivity than carbon so a conclusion must be it is the thermal conduction through the thickness of the material must also have an effect. Moreover, the entire nature of the laminate will have an effect and therefore it could be assumed that the response from a laminated composite will be not just a result of the ply lay-up, the resin rich layer or a combination of both but the ply thickness and even manufacturing method. The material used in [15] had much thicker plies and a room temperature cure. The thicker plies and the consolidation which resulted in a volume fracture of fibres of between 40 and 50% served to minimised through-thickness heat transfer, and encouraged adiabatic conditions. It was shown there was little variation in thermoelastic response with loading frequency regardless of the layup. The thin plies and autoclave cure, i.e. 0.125 mm, of the prepreg used in the current work produced a volume fraction of 56%. These allow heat transfer to occur and therefore provide the homogenising effect, at low loading frequencies,

which necessitates the implementation of the global calibration approach for application to larger panels in the loading rig.

It is known [11] that the effects of heat transfer within a lamina, due to its heterogeneity, can be dismissed. Therefore the variation in thermoelastic response with loading frequency, demonstrated in Figs. 3 and 4, must be an artefact of interlaminar heat transfer. Hence, at low cyclic frequencies, i.e. as with 1 Hz applied with the pressure test rig, the measured thermoelastic response has been homogenised. It is hypothesised that application of the global calibration approach described above will ameliorate the non-adiabatic behaviour and allow useful results to be obtained from the TSA at low cyclic loads; this is investigated in the next section. The variation in thermoelastic constant with both loading frequency and laminate layup indicates that the thermoelastic constant must be obtained experimentally for laminated composite structures from calibration specimens manufactured from identical materials, layup and at identical loading frequency to those used in full-scale tests. This conclusion is supported by the findings of [15] where different observations regarding the adiabatic behaviour were made because of the lamina thickness and material architecture.

FE Modelling Approach and Validation

The ultimate objective is to use TSA as a method to validate the predicted stress distribution from FE models. However, here, two models were constructed using ANSYS 11 (*ANSYS Inc, Canonsburg, USA*), which are used to better understand the mechanical and thermoelastic response of the structure. The first model type, referred to as the 'homogeneous model', treats the face sheet material as a homogeneous orthotropic block, whilst the second, referred to as the 'individual ply model', treats the face sheet as a laminated plate, i.e. considering the stresses ply by ply. The use of these two models enables an assessment of both the stress in the face sheet in terms of the global laminate, and also the stresses in the surface ply. The two modelling approaches correspond to the two calibration approaches; one treats the face sheet mechanically as whole, the other considers the coupling between the lamina in the face sheet. Clearly, treating the laminated materials as homogeneous blocks is an approximation, so verification is required to investigate the effect of such an approximation has on the ability of the model to predict the behaviour of the sandwich panel.

To investigate the effect of using the two methods for modelling the face sheets, CLT [16] was used, again, to calculate the stiffness matrices, A, B and D [16], of the two generic panels, QI and CP. Hence, determining if neglecting the coupling in the simpler homogeneous model has an effect on the predicted deflections. The material properties of the constituent parts of the panels are presented in Table 6. Where possible these have been measured experimentally, but some have been taken from literature or estimated. The inaccuracies in these properties are not expected to sufficiently affect the comparison between the model and TSA data. The stiffness matrices relate the stresses and strains as follows [16]:

$$\begin{bmatrix} N \\ M \end{bmatrix} = \begin{bmatrix} A & B \\ B & D \end{bmatrix} \times \begin{bmatrix} \varepsilon^0 \\ \kappa^0 \end{bmatrix} \tag{6}$$

where N are loads, M are moments, are ε^0 strains and κ^0 are the curvatures on the reference plane.

The lay-up of the panels was symmetrical, and therefore there is no need to calculate the B matrix which would be unpopulated for a symmetric laminate. The stiffness matrices for the QI panel using the homogeneous FE model are as follows:

$$A = \begin{bmatrix} 14.89 & 0.19 & 0 \\ 0.19 & 15.39 & 0 \\ 0 & 0 & 2.02 \end{bmatrix} \times 10^{10}, \tag{7}$$

$$D = \begin{bmatrix} 669.56 & 8.25 & 0 \\ 8.25 & 692.85 & 0 \\ 0 & 0 & 90.67 \end{bmatrix} \times 10^{10}$$

Table 6 Material properties of honeycomb core and carbon fibre face sheets for FE models

Property	Core	Individual ply	Quasi-isotropic Homogeneous	Cross ply Homogeneous
E_x (Pa)	400.0×10^6	134×10^9	48.7×10^9	71.8×10^9
E_y (Pa)	400.0×10^6	9.0×10^9	50.4×10^9	71.8×10^9
E_z (Pa)	400.0×10^6	9.0×10^9	9.0×10^9	9×10^9
ν_{xy}	0.30	0.32	0.09	0.03
ν_{yz}	0.30	0.09	0.15	0.03
ν_{xz}	0.30	0.09	0.15	0.3
G_{xy} (Pa)	59.3×10^6	6.6×10^9	6.6×10^9	6.6×10^9
G_{yz} (Pa)	32.4×10^6	6.6×10^9	6.6×10^9	6.6×10^9
G_{xz} (Pa)	32.4×10^6	6.6×10^9	6.6×10^9	6.6×10^9

The stiffness matrices for the QI panel using the individual ply FE model are as follows:

$$A = \begin{bmatrix} 14.89 & 0.19 & 0 \\ 0.19 & 15.39 & 0 \\ 0 & 0 & 2.02 \end{bmatrix} \times 10^{10}, \quad (8)$$

$$D = \begin{bmatrix} 669.56 & 8.25 & 0 \\ 8.25 & 692.85 & 0 \\ 0 & 0 & 90.67 \end{bmatrix} \times 10^{10}$$

The A matrix contains extensional stiffnesses (in-plane laminate moduli) that relate to in-plane loads and in-plane strains. Therefore, differences found in the A matrix will be insignificant for the bending dominant load situation considered in this work. The D matrix contains bending and twisting laminate stiffnesses relating moments to curvature. The D matrix shows the major difference between the two modelling approaches. The D matrix for the homogeneous model has zero values for bend-twist coupling stiffness, whilst for the individual ply model these stiffnesses have large values. It is known [16] that a laminate with a cross-ply configuration has no torsion coupling. For the panel with the CP face sheets the values of the bend-twist coupling stiffnesses in matrix D for both models are zero i.e. for the homogeneous model:

$$A = \begin{bmatrix} 21.79 & 0.07 & 0 \\ 0.07 & 21.79 & 0 \\ 0 & 0 & 2.02 \end{bmatrix} \times 10^{10}, \quad (9)$$

$$D = \begin{bmatrix} 948.98 & 2.77 & 0 \\ 2.77 & 984.98 & 0 \\ 0 & 0 & 90.07 \end{bmatrix} \times 10^{10}$$

and also for the individual ply model:

$$A = \begin{bmatrix} 10.78 & 0.32 & 0 \\ 0.32 & 10.78 & 0 \\ 0 & 0 & 0.99 \end{bmatrix} \times 10^{10}, \quad (10)$$

$$D = \begin{bmatrix} 492.97 & 14.52 & 0 \\ 14.52 & 490.32 & 0 \\ 0 & 0 & 45.15 \end{bmatrix} \times 10^{10}$$

As the bend-twist stiffness terms are zero in both cases there should be no difference between the stress and deflection predictions made using the two different modelling approaches for the CP panel.

In previous work [10] a homogeneous model was constructed to enable the design of the pressure rig. This approach was adopted again in the current paper. The model uses Shell181 for the face sheet; a four node element suitable for producing layered FE models, which is essential for the individual ply model. The element can also accommodate large linear rotations and large nonlinear strains, therefore enabling the out-of-plane displacement of the panel to be derived. The core was assumed to be a single anisotropic solid volume with material properties as given in Table 6 (taken from the manufacturer's data sheet), modelled using Solid185; an eight node brick element. It should be noted that the in plane properties of the core were assumed to be isotropic. This is a gross assumption but the majority of the load is carried in shear in the core and hence the values of shear stiffness used (see Table 6) reflect the orthotropic nature of the core. This was considered a better approach than to use literature values for the in plane properties which will not reflect accurately the actual core properties. The model was meshed with elements of 0.01 m producing a mesh density shown in Fig. 5. For simplicity the bolted constraints in the rig were neglected and represented by imposing zero deflection on three edges of the model; i.e. the two short edges and one of the longer edges. With such boundary conditions, the model is constrained in all degrees of freedom along three edges, whilst the free edge has six degrees of freedom. A pressure load of 0.0103 MPa was applied to the model, equal to that used during the tests, by applying a force perpendicular to each of the 2150 surface nodes. The pressure equates to a load of 0.96 N per node. The model is relatively thin in comparison to its length and width, and is subjected to an out-of-plane pressure load that would induce relatively large deflections. For this reason the model was solved using a geometrically nonlinear solver. Figure 5 shows the FE mesh alongside an example of the contour plot of the out of plane deflection of the model when subjected to a load of 0.0103 MPa.

The individual ply model was developed using the capability of Shell181 to produce laminated structures. The model was the same as the homogeneous, with the

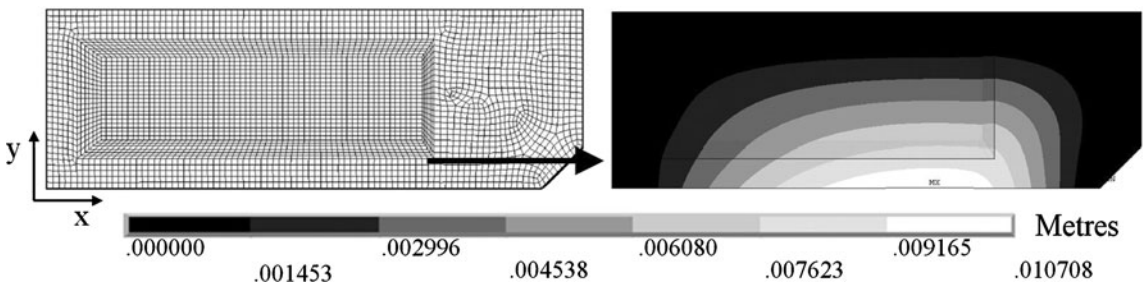

Fig. 5 FE model mesh density and representative contour plot of predicted out-of-plane displacement

exception of the treatment of the face sheets. The face sheets were built up from 24 'individual plies' with the corresponding layup for the QI and CP panels. Over the shaped section of the core the fibre orientation was maintained by altering the individual element coordinate systems such that the z-axis remained perpendicular to the surface. The face sheet properties for each model are provided in Table 6.

The measured deflection from the LVDT was compared to the predicted maximum deflection to provide a validation of the two modelling approaches applied to both the QI and CP panels. Table 7 lists the measured maximum deflection for the two panels, alongside that predicted by the two types of FE model. For the panel with the QI face sheet the predicted deflection from the two models differ by 2 mm; the experimental deflection sits in between the two values. In the panel with the CP face sheets both FE models provide practically identical deflections, confirming that the bend-twist coupling effect causes the difference in the predicted deflections for the QI face sheet panel. Most importantly here the measured deflection is very close to that given by the model and provides a validation of the modelling procedure. The stress data from the two types of validated FE model was then processed into a form that is comparable to the experimental TSA data using the thermoelastic constants derived in the previous section. This allowed the use of the predicted stress data to further investigate the nature of the TSA response from the QI and CP panels.

Thermoelastic Data Analysis

The ΔT from the TSA applied to the panels and stresses from the FE models were manipulated into the form in (equation (3)) using both the UD and global values of K to provide a comparable stress metric. To investigate the effectiveness of the global calibration approach the K_x and K_y were applied to the homogeneous FE model as shown in (equation (3)). Figure 6 shows the full-field data for the CP panel for the global calibration, as an example, although the results for the QI panel are very similar. Figure 6a and b show the result of using the experimental derived global

Table 7 Maximum deflection data for the generic panels experimentally measured and predicted

Panel	Experimental (mm)	FE Homogeneous (mm)	FE Individual ply (mm)
QI	6.34	7.70	5.70
CP	7.03	7.11	7.13

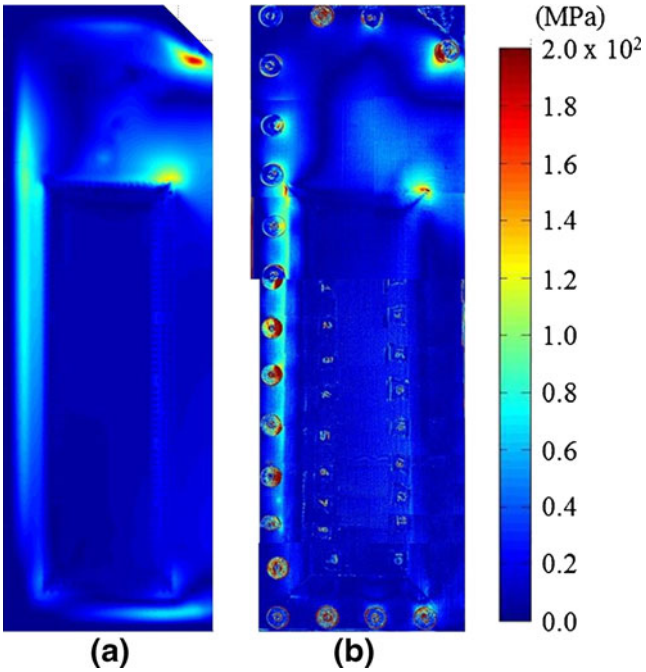

Fig. 6 CP panel calibration using global approach (**a**) homogeneous FE model, (**b**) TSA

calibration constants on the homogeneous FE model and TSA data respectively. Setting aside the difference at the bolted connections, the stress distribution appears to be in very good agreement between the homogeneous FE model data and the TSA in terms of both the magnitude and distribution. To provide a quantitative comparison of the calibrated stress metrics, a line of data is plotted through the stress concentration at the top right corner of the core (see arrow on Fig. 5) for each of the data sets and relevant calibration approach. Figure 7a shows the line plots from the TSA and the FEA for the CP panel calibrated using the global approach. Comparing the peak stress metric values, at a position of around 50 mm, the FE predicts a peak value of approximately 130 MPa, and experimentally the TSA gives 150 MPa. Therefore the homogeneous FE model under predicts the stress metric peak by only 15%, which could be attributed to the relatively course FE mesh cropping the peak. The data shown in Fig. 7a provides an encouraging indication that using the global thermoelastic constants, derived from experiments at the actual loading frequency, is a valid means of obtaining quantitative stress metric values from non-adiabatic thermoelastic data. Furthermore, the results also confirm, that by loading at low cyclic frequencies a homogenising effect of the thermal characteristics of each ply has occurred facilitating the application of the global calibration approach. To further confirm the validity of the global calibration approach, Fig. 7b plots line data from the QI panel for the homogeneous FE model and TSA

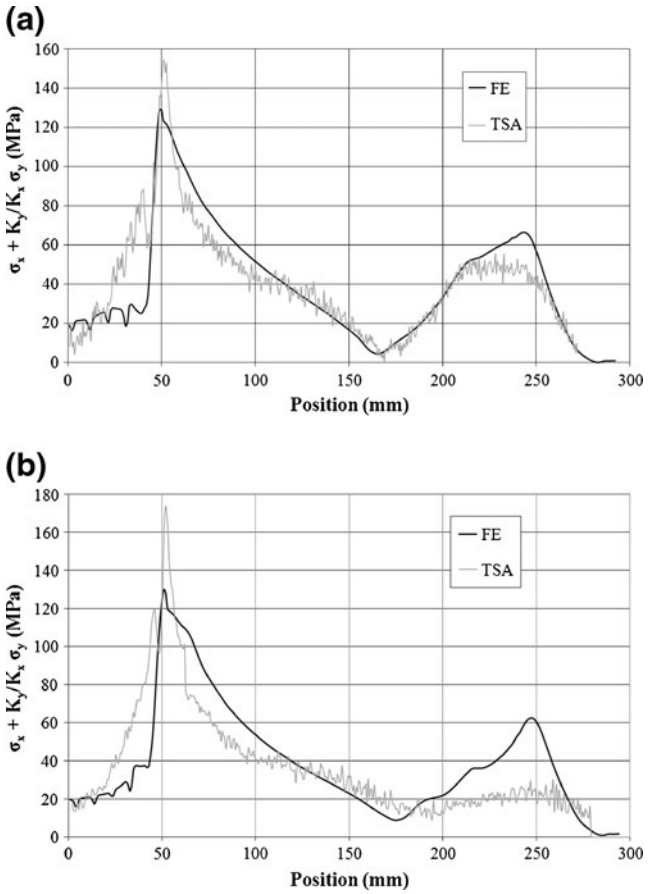

Fig. 7 Line plot comparison of FE and TSA for (**a**) CP panel calibrated using global approach, (**b**) QI panel calibrated using global approach

data calibrated with the global approach. Here the agreement between the two data sets is also very good, apart from the right hand side where the bolted connection is affecting the experimental data. Once again the TSA gives a greater peak reading at the stress concentration because the course mesh density cannot capture the peak. Figure 7b provides further evidence to support the conclusion that the global calibration approach can provide a means of deriving useful stress data from the thermoelastic response even if non-adiabatic conditions prevail.

To establish if the UD calibration approach provides meaningful results Fig. 8a and b show the results of the UD calibration on the individual ply FE model and TSA data for the CP panel. Here it is difficult to discern any agreement between the FE data set and the TSA data. The distribution and value of the stresses predicted are very different to the measured data. Figure 9a provides line plots for the CP panel data calibrated using the UD approach. Using the peak stress metric at the same point for comparison, the individual ply model predicts approximately 3200 MPa and experimentally the TSA measured 1400 MPa. When using the UD calibration approach, paired with the individual ply FE model, the predicted stress metric is much larger than the measured value. For a final confirmation of the inability of the UD calibration to provide comparable stress metrics between the FE and TSA data, Figure 9b plots the individual ply FE model and TSA data calibrated with the UD approach for the QI panel. The line demonstrates the same trend as the CP panel; the FE provides a huge overestimation of the stress metric in comparison to the TSA.

The observations above point towards a restriction in the application of the UD calibration approach at low cyclic frequencies. The possibility is that the surface ply is affected

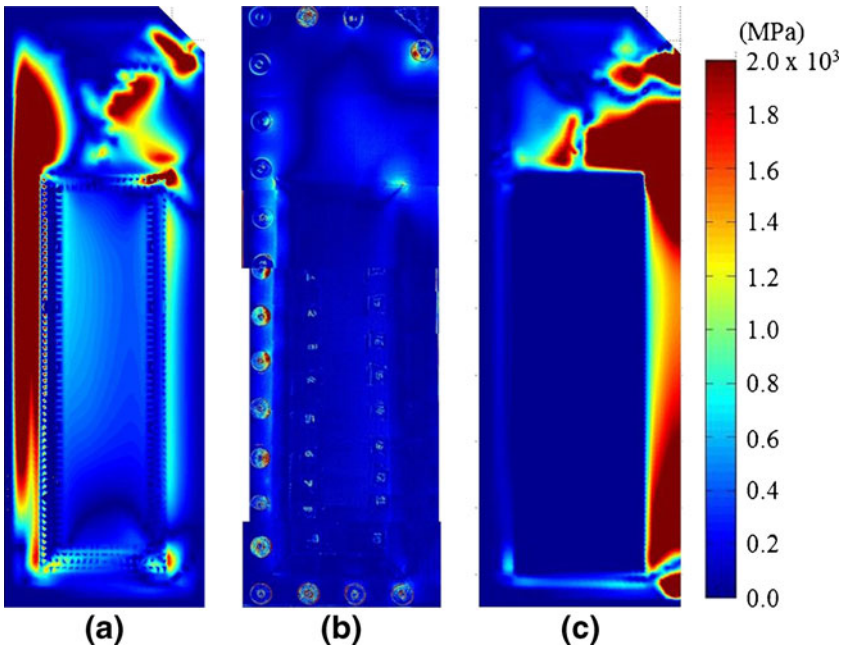

Fig. 8 CP panel calibration using UD approach (**a**) individual ply model, (**b**) TSA, (**c**) UD calibration applied to second ply

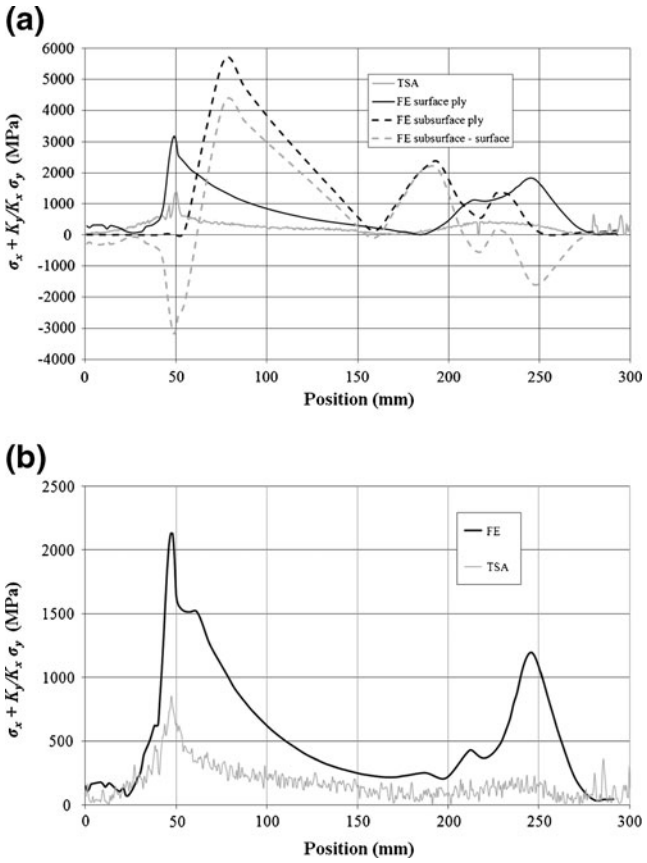

Fig. 9 Line plot comparison of FE and TSA for (**a**) CP panel calibrated using UD approach, (**b**) QI panel calibrated using UD approach

by non-adiabatic behaviour, as heat is transferred between plies. Figure 4a shows data from the tensile specimens where the non-adiabatic behaviour causes departures in the thermoelastic response at 1 Hz for a 0^o surface ply the thermoelastic response of the CP specimen is about 2.5 times greater that of the UD specimen and the QI is less but around twice that of the UD. The plots in Fig. 4 show that the UD material does not suffer from the same non adiabatic behaviour because the stress induced temperature change does not vary ply by ply. Therefore at 1 Hz the UD calibration does not account for the non-adiabatic behaviour. In the panels it is appropriate to examine the stresses in the sub surface plies to ascertain if there is sufficient difference in the stresses ply by ply to drive non-adiabatic behaviour. Figure 8c shows the calibration applied to the subsurface ply. Here it is clear that the thermoelastic response from the surface and subsurface ply are very different. Figure 9a shows the data, along the usual line, for the subsurface and also plots the difference between the two. The difference is marked and therefore it cannot be assumed that the response is adiabatic. However applying the UD calibration to the surface ply alone does assume this, and that the surface ply is thermally isolated from the rest of the specimen. Clearly at these low loading frequencies using the UD calibration approach is not appropriate. Furthermore examining the peak value to the left of the plot it can be seen that the difference in the FE and TSA data is approximately the same as that seen between the UD and CP calibration constants seen in Fig. 4a.

To finalise this discussion it would be desirable to conduct tests on the panels at 20 Hz where the UD calibration constants converge according to Fig. 4. However, with the available equipment this is not possible. Most standard servo-hydraulic test machines cannot cope with large displacements at high frequencies. An impractical redesign would be required that uses a very large pump (current pump provides 70 l/s) or large accumulator as used in very high strain rate test machines. Therefore the current work has shown a way of applying thermoelastic stress analysis to laminated materials at low frequencies that accounts for the non-adiabatic response.

Conclusions

A method for assessing large carbon fibre sandwich panels has been established using TSA. To ensure adiabatic conditions in a composite material it is usual to apply a cyclic load of at least 10 Hz. However, by obtaining calibration constants from tensile strips loaded at 1 Hz it was shown that it is possible to process full-field TSA data from a large representative carbon fibre sandwich panel loaded at just 1 Hz. The TSA data and stresses from two types of FE model were processed into a form that was comparable using two calibration approaches. The first used values measured from composite specimens manufactured from the same lay-up as the face sheets of the generic panel, whilst the second used values measured from UD composite tensile specimens. The UD calibration approach applied to the surface ply is known to work for situations where the surface ply can be treated in thermal isolation, however when applied to a more complex loading case the UD calibration does not adequately model the thermomechanics of the panel. However, it has been shown that the global calibration produces results that fit well to a homogeneous FE model. The results are very encouraging in the sense that the idea of calibrating at the actual loading frequency provides a means of interpreting thermoelastic data from components that are subject to non-adiabatic behaviour.

Acknowledgements The authors are grateful to GE Aviation and particularly Mr John Savage for supporting this work. The support of the technicians in the University of Southampton Engineering Design and Manufacturing Centre and the Transport Systems Research Laboratory in the design and commissioning of the test rig is also gratefully acknowledged.

References

1. Stanley P, Chan WK (1988) The application of thermoelastic stress analysis to composite materials. J Strain Anal Eng 23(3):137–142
2. Diaz FA, Patterson EA, Tomlinson RA, Yates JR (2004) Measuring stress intensity factors during fatigue crack growth using thermoelasticity. Fatig Fract Eng M 27(7):571–584
3. Lin ST, Miles JP, Rowlands RE (1997) Image enhancement and stress separation of thermoelastically measured data under random loading. Exp Mech 37(3)
4. El-Hajjar R, Haj-Ali R (2003) A quantitative thermoelastic stress analysis method for pultruded composites. Compos Sci Tech 63 (7):967–978
5. Emery TR, Dulieu-Barton JM, Earl J, Cunningham PR (2008) A generalised approach to the calibration of orthotropic materials for thermoelastic stress analysis. Compos Sci Tech 68(3–4):743–752
6. Paynter RJH, Dutton AG (2003) The use of a second harmonic correlation to detect damage in composite structures using thermoelastic stress measurements. Strain 39(2):73–78
7. Dulieu-Smith JM, Quinn S, Shenoi RA, Read PJCL, Moy SSJ (1997) Thermoelastic stress analysis of a GRP tee joint. Appl Compos Mater 4(5):283–303
8. Crump DA, Dulieu-Barton JM, Savage J (2010) The manufacturing procedure for aerospace secondary sandwich structure panels. J Sandw Struct Mater 12, doi:1099636208104531
9. Johannes M, Dulieu-Barton JM, Bozhevolnaya E, Thomsen OT (2008) Characterisation of local effects at core junctions in sandwich structures using thermoelastic stress analysis. J Strain Anal Eng Des 43(6):469–492
10. Crump DA, Dulieu-Barton JM, Savage J (2010) Design and commission of an experimental test rig to apply a full-scale pressure load on composite sandwich panels representative of an aircraft secondary structure. Meas Sci Tech, 21, p 16, doi:1088/0957-0233/21/1/015108
11. Wong AKL (1991) A non-adiabatic thermoelastic theory for composite laminates. J Phys Chem Solid 52(3):483–494
12. Crump DA, Dulieu-Barton JM (2010) Analysis of large scale composite components using TSA at low cyclic frequencies. In: SEM Annual conference and exposition on experimental and applied mechanics
13. Sambasivam S, Quinn S, Dulieu-Barton JM (2009) Identification of the source of the thermoelastic response from orthotropic laminated composites. 17th International Conference on Composite Materials (ICCM17), Edinburgh, 11 pages on CD
14. Sambasivam S (2009) Thermoelastic stress analysis of laminated composite materials. University of Southampton, Faculty of Engineering, Science and Mathematics, Doctoral Thesis
15. Pitarresi G, Galietti U (2010) A quantitative analysis of the thermoelastic effect in CFRP composite materials. Strain 46(5):446–459
16. Daniel IM, Ishai O (1994) Engineering mechanics of composite materials. Oxford University Press
17. Pitarresi G, Found MS, Patterson EA (2005) An investigation of the influence of macroscopic heterogeneity on the thermoelastic response of fibre reinforced plastics. Compos Sci Tech 65:269–280
18. Shimazaki Y, Hojo F, Takezawa Y (2008) Preparation and characterization of thermoconductive polymer nanocomposite with branched alumina nanofiber. Appl Phys Lett 92
19. Kalogiannakis G, Van Hemelrijck D, Van Assche G (2004) Measurements of thermal properties of carbon/epoxy and glass/epoxy using modulated temperature differential scanning calorimetry. J Compos Mater 38(2):163–175
20. Cease H, Derwent PF, Diehl HT, Fast J, Finley D (2006) Measurement of mechanical properties of three epoxy adhesives at cryogenic temperatures for CC construction. Fermilab-TM-2366-A